

The low-energy cosmic X-ray background spectrum observed by the BeppoSAX LECS

A.N. Parmar¹, M. Guainazzi¹, T. Oosterbroek¹, A. Orr¹, F. Favata¹, D. Lumb¹, and A. Malizia^{2,3}

¹ Astrophysics Division, Space Science Department of ESA, ESTEC, Postbus 299, 2200 AG Noordwijk, The Netherlands

² BeppoSAX Science Data Center, Nuova Telespazio, via Corcolle 19 I-00131 Roma, Italy

³ Department of Physics and Astronomy, Southampton University, SO17 1BJ, UK

Received 1998 December 9; Accepted 1999 March 5

Abstract. The spectrum of the 0.1–7.0 keV cosmic X-ray background (CXB) at galactic latitudes $>|25|^\circ$ has been measured using the BeppoSAX Low-Energy Spectrometer Concentrator (LECS). Above 1 keV the spectrum is consistent with a power-law of photon index 1.47 ± 0.10 and normalization 11.0 ± 0.8 photon $\text{cm}^{-2} \text{s}^{-1} \text{keV}^{-1} \text{sr}^{-1}$ at 1 keV. The overall spectrum can be modeled by a power-law with 2 thermal components, or by a broken power-law and a single thermal component. In both cases the softer thermal emission dominates $\lesssim 0.3$ keV and is seen through a column, N_{H} , of a few 10^{19} atom cm^{-2} . The other components have N_{H} consistent with the mean line of sight value. The metal abundances for the thermal components are poorly constrained, but consistent with cosmic values. The power-law together with 2 thermal components model has been used to fit recent combined ASCA and ROSAT CXB measurements. Here, the soft thermal component is interpreted as emission from the local hot bubble and the hard thermal component as emission from a more distant absorbed region. While such a 2 component thermal model is consistent with the LECS spectrum, it is not *required*, and the hard thermal component may result from inadequate modeling of the extragalactic contribution. The observed low-energy spectral complexity may therefore originate primarily in the local hot bubble. There is no evidence for the presence of a very soft CXB component with a temperature $\lesssim 0.1$ keV. The emission measure seen by ROSAT is rejected at 90% confidence.

Key words: ISM: atoms – ISM: bubbles – ISM: general – diffuse radiation – X-rays: ISM

1. Introduction

The diffuse Cosmic X-ray Background (CXB) was discovered in 1962 predating the discovery of the Cosmic Microwave Background (CMB) by several years.

Send offprint requests to: A.N.Parmar (aparmar@astro.estec.esa.nl)

The spectral characteristics and the spatial distribution of the CXB have been measured by many X-ray missions, but its origin is still not yet fully understood. The 3–60 keV spectrum is well described by a thermal bremsstrahlung model with a temperature, kT, of 40 keV (Marshall et al. 1980). Between 1 and 10 keV this shape can be approximated by a power-law with a photon index, α , of 1.4 (Jahoda et al. 1992; Gendreau et al. 1995). The lack of distortion of the CMB expected from a truly diffuse hot intergalactic medium supports the idea that the CXB above 1 keV is dominated by emission from an unresolved distribution of active galactic nuclei (AGN; Setti & Woltjer 1989; Madau et al. 1993; Comastri et al. 1995). Recent results from the deepest (flux limit $\sim 10^{-15}$ erg $\text{cm}^{-2} \text{s}^{-1}$) X-ray survey so far performed, suggest that the fraction due to discrete sources in the energy range 0.5–2.0 keV is 70–80% (Hasinger et al. 1998). Recent results from a BeppoSAX survey support such an origin (Fiore et al. 1998).

Below ~ 1.5 keV the CXB shows additional spectral and spatial complexity. Spatially, there is a large degree of structure visible, with several features evident in all-sky maps (e.g. McCammon & Sanders 1990; Snowden et al. 1995). At ~ 0.25 keV there is a clear anti-correlation with both galactic latitude (the CXB being significantly weaker at the galactic equator), and with the amount of HI in the line of sight (Snowden et al. 1994). The low-energy CXB spectrum deviates from the simple power-law observed $\gtrsim 1$ keV. Line emission from O VII and C V was observed using solid-state detectors by Rocchia et al. (1984) and Inoue et al. (1980), strongly supporting the view that emission from an optically thin thermal plasma contributes significantly at low-energies. Later studies (e.g., Kerp et al. 1993) show that to fit ROSAT Position Sensitive Proportional Counter (PSPC) spectra of the soft CXB two thermal components are required, in addition to the power-law.

The spatial dependence of the low-energy CXB is similar to that expected if extragalactic, isotropic emission is absorbed by the galactic interstellar medium (ISM). However, the observed degree of modulation of

the CXB and the lack of a significant spectral modulation (McCammon et al. 1983) are incompatible with such a model. Thus, a significant part of the soft CXB emission is likely to be of local origin. Models which rely on a significantly clumpy ISM (Jakobsen & Kahn 1986) have been proposed to explain the lower than expected modulation from an isotropic ISM. Diffuse emission maps and deeper pointed observations of shadowing by cold gas (Snowden et al. 1997; Kerp 1994; Kerp et al. 1999) have revealed a consistent yet complex origin for the diffuse background. A soft (~ 0.1 keV) component originates from a combination of the local hot bubble and a galactic halo, but with the latter modulated spatially by local enhancements from bright clouds. In the 0.75 keV energy range the galactic emission is dominated by a bulge component and other enhancements associated with relatively nearby supernova remnants and wind-blown bubbles, together with a galactic plane enhancement of which some component is undoubtedly due to a superposition of individual sources. There may also be a contribution from inter-cluster gas of the Local Group (see Hasinger 1996 and references therein).

Deep pointed observations performed with imaging detectors onboard ROSAT and ASCA have provided a good opportunity to study the 0.1–10 keV CXB, typically yielding, as discussed above, a spectrum compatible with a power-law and two thermal components. However, the spectral parameters derived from the two missions are not always consistent. In particular, the power-law slopes are not always in agreement (see the discussion in Chen et al. 1997) and even in the well calibrated 1–2 keV overlapping energy range, estimates of the CXB flux vary by 15–20%. Even measurements using the same instrument (the PSPC) differ significantly in spectral parameters (cf. Hasinger 1992 and Georgantopoulos et al. 1996).

2. The instrument and observations

The Low-Energy Concentrator Spectrometer (LECS; 0.1–10 keV; Parmar et al. 1997) is an imaging gas scintillation proportional counter on-board the Italian-Dutch BeppoSAX X-ray astronomy mission (Boella et al. 1997). In comparison with the 0.1–2.5 keV PSPC, the LECS offers energy resolution a factor ~ 2.4 better and an extended high-energy response, overlapping with the ASCA Solid State Imaging Spectrometer (SIS; 0.5–10 keV). The LECS has comparable energy resolution to the SIS at ~ 0.5 keV. This combination of moderate energy resolution and broad energy coverage provides a unique capability for studying the low-energy CXB. In particular, the determination of the normalization and break energy of the CXB spectrum around 1 keV has proved problematical. The LECS spans this energy range exactly and so provides the potential for accurately measuring the relative contributions of the galactic and extragalactic components.

The LECS has a circular field of view (FOV) of 37' diameter (Parmar et al. 1997) and an effective area of ~ 10 cm² at 0.28 keV and ~ 40 cm² at 2 keV. In the central 8' radius of the FOV, the mean Non X-ray Background (NXB) 0.1–10 keV counting rate is 5.2×10^{-6} s⁻¹ keV⁻¹ arcmin⁻² (Parmar et al. 1999). The 1.25 μ m thick LECS entrance window is supported by a fine grid and a strongback. The strongback divides the aperture into 4' \times 4' squares, each of which is divided into a matrix of 8 by 8 squares by the fine grid. The obscuration caused by the fine grid is energy independent and does not vary significantly with FOV position. In contrast, the strongback produces a position dependent obscuration which is also slightly energy dependent due primarily to the variation of the mirror point spread function with energy (Parmar et al. 1997).

A 559 ks exposure background spectrum was accumulated from a number of high galactic latitude exposures by extracting counts within an 8' radius of the nominal source position within the LECS FOV (Table 1). The choice of background fields and LECS background subtraction methods are discussed in Parmar et al. (1999). The background fields were selected to avoid any of the obvious brightness enhancements in the ROSAT maps in order to provide a reliable estimate of the spectrum at “typical” locations out of the galactic plane. The CXB spectrum is expected to include contributions from emission in the local hot bubble, the galactic halo, and unresolved AGN.

No point sources are present in the individual fields with 0.1–2.0 keV fluxes $> 1.7 \times 10^{-13}$ erg cm⁻² s⁻¹. The background spectrum includes contributions from the CXB, the NXB (which is internal to the instrument), and any X-rays from within a solid angle of 2° which may undergo a single reflection and be detected in the FOV (Conti et al. 1994). The extraction region was chosen to include 95% of the 0.28 keV X-rays and is the region where the instrument is best calibrated. All the fields have galactic latitudes of $> |25^\circ|$ and Galactic column densities of between 2.0 and 7.0×10^{20} atom cm⁻².

The contribution of the NXB was subtracted using a 499 ks NXB spectrum accumulated during intervals of dark Earth pointing. The properties of this spectrum are discussed in Parmar et al. (1999). Briefly, in the central 8' the LECS NXB spectrum is approximately constant with energy with a count rate of 8×10^{-4} s⁻¹ keV⁻¹. Above ~ 4 keV there is a smooth increase in count rate with 3 discrete line features superposed. In the energy ranges 0.1–0.5 keV, 0.5–2.0 keV and 2.0–5.0 keV the NXB contributes 13%, 19%, and 47% of the total background, respectively. Above ~ 8 keV, the NXB dominates the overall background spectrum. The LECS NXB shows a gradual reduction in counting rate by $\sim 15\%$ over an interval of ~ 2 years (Parmar et al. 1999). Due to the low-inclination, almost circular, BeppoSAX orbit, variations in the NXB counting rate around the orbit are negligible.

Table 1. LECS observations used to create the CXB spectrum. A target name including “sec” or “secondary” refers to the prime Wide Field Camera target in a direction orthogonal to the LECS pointing. N is the number of individual pointings. N_{gal} is the line of sight absorption in units of 10^{20} atom cm^{-2} (Dickey & Lockman 1990)

Target	Observation		N	LECS Pointing (J2000)		l_{II} ($^{\circ}$)	b_{II} ($^{\circ}$)	Exp. (ks)	N_{gal}
	Start (yr mn day)	Stop (yr mn day)		RA (h m s)	Dec ($^{\circ}$ ' ")				
Polaris Region	1996 Jul 01	1997 May 23	6	02 31 42.0	+89 15 47	123.3	+26.5	69.7	7.0
Gal cent-2 (sec)	1996 Aug 23	1996 Aug 27	1	16 51 19.5	+60 11 49	89.8	+38.1	82.3	2.1
Gal cent-3 (sec)	1996 Aug 27	1996 Aug 31	1	16 35 10.7	+59 46 30	89.9	+40.2	79.9	2.0
SGR-A (sec)	1996 Oct 10	1996 Oct 12	1	06 12 22.7	-60 59 04	270.1	-28.2	43.3	4.2
Secondary Target (S1)	1997 Mar 18	1997 Mar 25	1	17 56 46.1	+61 11 45	90.2	+30.1	94.2	3.4
Secondary Target (S2)	1997 Apr 13	1997 Apr 15	2	18 18 20.5	+60 58 42	90.2	+27.4	26.6	3.8
SDC Target	1997 Dec 13	1997 Dec 14	1	23 07 53.5	+08 50 06	84.4	-46.1	13.9	4.7
Secondary Target (S4)	1998 Mar 10	1998 Mar 22	2	05 52 07.9	-61 05 35	270.0	-30.6	46.7	5.3
Secondary Target (S5)	1998 Aug 22	1998 Oct 01	4	17 52 07.4	+61 01 01	89.9	+30.6	102.2	3.5

All data products were accumulated using the latest version of the LECS analysis software (SAXLEDAS 1.8.0). The spectrum was rebinned to have at least 20 counts per bin and to sample the full width half-maximum of the energy resolution with at most 3 energy bins, in order to ensure the applicability of the χ^2 statistic. All uncertainties are quoted at the 90% confidence level for one interesting parameter ($\Delta\chi^2 = 2.7$). When determining spectral uncertainties all the other variable parameters were allowed to vary freely. The photoelectric absorption coefficients of Morisson & McCammon (1983), together with the cosmic abundances of Anders & Grevesse (1989) were used (which are supposed to be representative of the composition of the proto-solar nebula). A response matrix appropriate for uniform diffuse emission was created using LEMAT 3.5.1. This matrix differs from the standard point-source response matrix in the following ways:

1. The nominal target position lies close to the center of a window support strongback square and the on-axis transmission is a factor 1.08 higher than the average for the entire extraction region.
2. The effects of off-axis mirror vignetting are included.
3. The CXB is modeled as a uniform diffuse emission, by means of 100 point sources randomly distributed within a radius of $12'$. This radius is larger than that of the extraction region ($8'$) to allow for photons from sources located within the region that are spread outside of the region by the finite detector resolution, and for events originating outside the extraction region which are spread inside.

In addition to the above effects, single reflected X-rays from within $120'$ can be detected in the FOV (Conti et al. 1994). In order to estimate the magnitude of this effect, 0.1–6 keV flux ratios between a pointed Crab Nebula observation (Cusumano et al. 1999) and two pointings where the Crab Nebula was located just outside

the LECS FOV, with offset angles of $45'$ and $60'$, were calculated. The spectrum of the singly reflected X-rays is consistent with that observed on-axis, but with a much reduced intensity. An exponential function was used to characterize the dependence of the flux ratios on offset angle. Assuming that the X-ray sky is uniform within $120'$, integration of this function reveals that singly scattered X-rays contribute $<1\%$ of the flux within an $8'$ extraction radius. Since this is well within the uncertainty in CXB normalization, this effect is ignored.

3. X-ray background spectrum

In the 1.0–7.0 keV energy range (at higher energies there is no signal at $>3\sigma$ and the LECS spectral calibration is more uncertain) a simple power-law fit gives an acceptable χ^2 of 39.0 for 44 degrees of freedom (dof) with $\alpha = 1.47 \pm 0.10$ and a normalization of 11.0 ± 0.8 photon $\text{s}^{-1} \text{cm}^{-2} \text{keV}^{-1} \text{sr}^{-1}$ at 1 keV. Significant excess counts are present in the spectrum at lower energies (see Fig. 1).

A good fit can be obtained in the 0.1–7.0 keV energy range with a low absorption ($N_{\text{H}} = 5 \times 10^{19}$ atom cm^{-2}) broken power-law, provided that a narrow (i.e. intrinsic width σ fixed at 0) Gaussian emission line is added to the continuum (model 1). The centroid energy implies that this feature is 0.57 keV K α emission from O VII, indicative of plasma at a temperature of ~ 0.1 keV. Best-fit parameters are listed in Table 2.

Following the current understanding of the CXB spectrum, the 0.1–7 keV LECS spectrum was next fit with a power-law together with a single temperature optically thin plasma (the Mewe-Kaastra-Liedhal plasma emissivity model in XSPEC, Mewe et al. 1985, 1986). This gives an unacceptable fit at $>95\%$ confidence ($\chi^2 = 83$ for 62 dof). An acceptable fit is obtained if an absorbed power-law is used, together with two thermal components with cosmic abundances (model 2). The N_{H} of the low

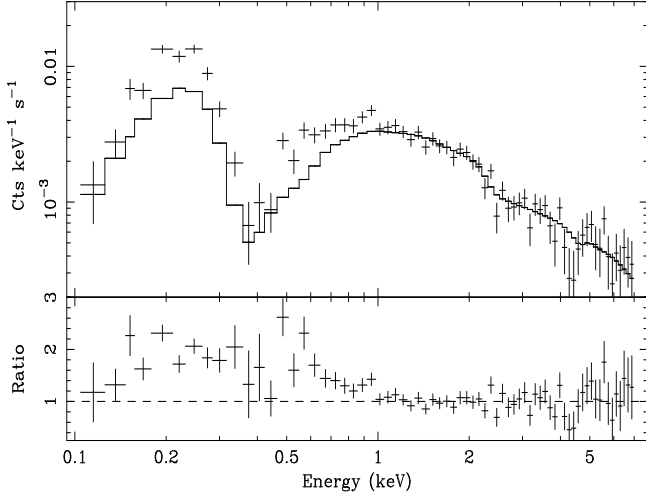


Fig. 1. Spectrum and residuals in units of the data/model ratio (lower panel), when the best-fit 1–7 keV power-law is extrapolated down to 0.1 keV

Table 2. Best-fit parameters for model 1 consisting of a broken power-law with a photon index α_{soft} below energy E_{break} and α_{hard} above. A narrow Gaussian line at an energy E_{line} with normalization I_{line} is included

Parameter	Value
Broken power-law	
N_{H} (10^{20} atom cm^{-2})	$0.5 \pm_{0.3}^{0.4}$
α_{soft}	2.03 ± 0.14
E_{break} (keV)	$1.4 \pm_{0.2}^{0.3}$
α_{hard}	1.43 ± 0.13
Gaussian line	
E_{line} (keV)	0.57 ± 0.05
I_{line} (ph cm^{-2} s^{-1})	$(6 \pm 4) \times 10^{-5}$
χ^2/dof	69.5/63

temperature thermal component was a free parameter in the fit, while the N_{H} of the other thermal and the power-law components was held fixed at the exposure weighted average of the galactic columns in the directions of each of the pointings listed in Table 1 (3.7×10^{20} atom cm^{-2}). The χ^2 is 66.5 for 63 dof (null hypothesis probability 36%). The addition of the second thermal component provides an improvement in fit quality at $>99.9\%$ confidence ($\Delta\chi^2 = 13.6$ for 2 dof). Fig. 2 shows a contour plot for the power-law spectral index versus normalization. The best-fit temperatures are $0.7 \pm_{0.3}^{0.2}$ keV and $0.137 \pm_{0.022}^{0.011}$ keV for the high and low absorption components, respectively (see Table 3).

The softer thermal component is observed through an absorbing column of 7×10^{19} atom cm^{-2} , consistent with the emission originating from ~ 50 pc (assuming a mean galactic plane local density of 0.4 atom cm^{-3} , Bloemen 1987). Fig. 3 shows the observed spectrum and best-fit model obtained using the parameters listed in Ta-

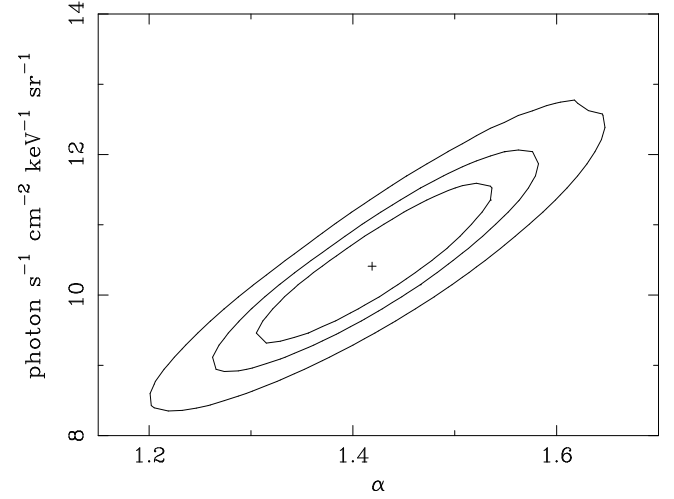


Fig. 2. Iso- χ^2 contours for the power-law normalization versus spectral index using model 2. Contours correspond to $\Delta\chi^2 = 2.3, 4.6$ and 9.2

Table 3. Best-fit parameters for model 2 consisting of a power-law and two thermal plasmas. Abundances are fixed at cosmic values. The absorption of the power-law and hard thermal components was fixed at the mean line of sight value. The values in square brackets are the one-sided variations in best-fit values when N_{H} is fixed at 2.0 and 7.0×10^{20} atom cm^{-2} . The power-law normalization is in units of photon cm^{-2} s^{-1} keV^{-1} sr^{-1} at 1 keV

Parameter	Value
Power-law	
N_{H} (10^{20} atom cm^{-2})	3.7
α	1.42 ± 0.10 [0.02]
Normalization	$10.4 \pm_{1.1}^{1.4}$ [0.3]
“Soft” thermal	
kT (keV)	$0.137 \pm_{0.022}^{0.011}$ [0.002]
Normalization (ph cm^{-5})	$(2.6 \pm_{0.6}^{1.4}) \times 10^{-4}$ [0.3]
Abundance	0.04–9.5
N_{H} (10^{20} atom cm^{-2})	$0.7 \pm_{0.3}^{0.4}$ [0.1]
“Hard” thermal	
kT (keV)	$0.7 \pm_{0.3}^{0.2}$ [0.03]
Normalization (ph cm^{-5})	$(3.1 \pm 1.4) \times 10^{-5}$ [0.5]
N_{H} (10^{20} atom cm^{-2})	3.7
χ^2/dof	66.5/63

ble 3. The soft component is responsible for the majority of the oxygen line emission evident in the spectrum. The 1–2 keV CXB flux is 1.47×10^{-8} erg cm^{-2} s^{-1} sr^{-1} . The ratio between the fluxes of the thermal and non-thermal components in the 0.5–2.0 keV energy range is 0.55.

The quality of the data is not sufficient to strongly constrain the abundances of the plasmas responsible for the thermal emission. Leaving the metal abundances free to vary does not result in a significant improvement in fit quality. In particular, the abundance of the hotter compo-

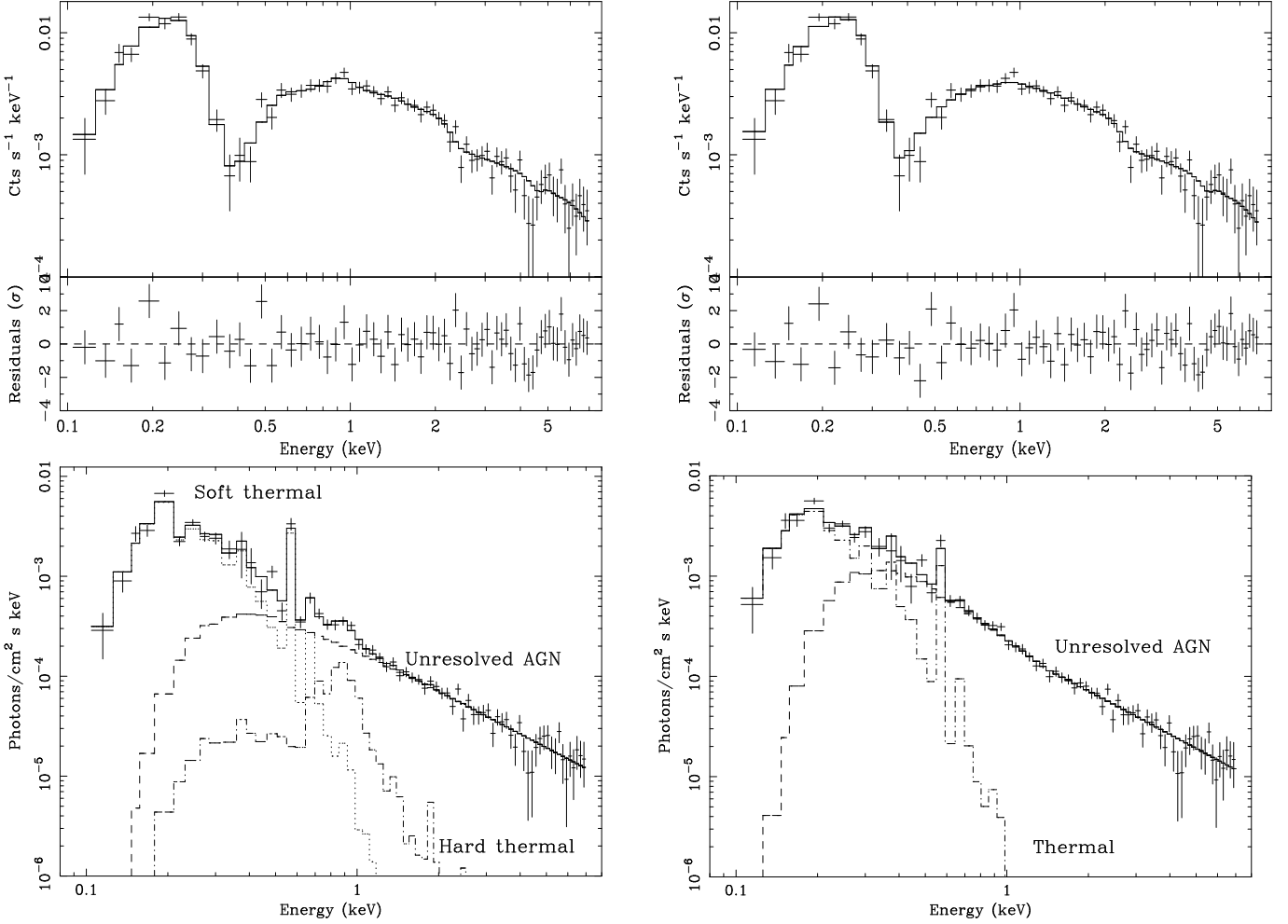


Fig. 3. The left panels show the power-law and two thermal model fit (model 2; Table 3). The right panels show the broken power-law and single thermal model fit (model 3; Table 4). Observed spectra are shown in the upper panels, fit residuals in units of standard deviations in the middle panels and the unfolded spectra in the lower panels

Table 4. Best-fit parameters for model 3 consisting of a broken power-law and a single thermal component. The abundance is fixed at cosmic values. The broken power-law N_{H} was fixed at the mean line of sight value and its normalization has units of photon $\text{cm}^{-2} \text{s}^{-1} \text{keV}^{-1} \text{sr}^{-1}$ at 1 keV

Parameter	Value
Broken power-law	
N_{H} (10^{20} atom cm^{-2})	3.7
α_{soft}	2.1 ± 0.3
α_{hard}	1.46 ± 0.14
Break energy (keV)	1.4 ± 0.4
Normalization	12.7 ± 0.6
Thermal	
kT (keV)	0.12 ± 0.02
Normalization (ph cm^{-5})	$(2.0 \pm 1.3) \times 10^{-4}$
N_{H} (10^{20} atom cm^{-2})	0.5 ± 0.5
χ^2 / dof	70.0/63

ment is essentially unconstrained. For the soft component the abundance can be constrained to be between 0.04 and 9.5 times cosmic values.

The summing of observations from regions of the sky with different amount of absorbing column can create artificial features in the spectrum, which may result in an incorrect estimation of spectral parameters. Therefore, the sensitivity of the derived spectral parameters to the assumed absorbing column density was investigated. N_{H} was fixed at the lowest and highest line-of-sight N_{H} values in Table 1 of 2.0 and 7.0×10^{20} atom cm^{-2} and the fit repeated. The changes in best-fit parameters are within their statistical uncertainties and shown in square brackets in Table 3. The same model was also applied to the spectra from the individual pointings. The temperature of the “hard” component is not well constrained, and was therefore fixed at its best-fit value given in Table 3. Again, none of the best-fit parameters differ from their average values by more than 1σ . This analysis indicates that the best-

fit spectral results are insensitive to the range of likely absorbing column densities.

An alternative spectral model, requiring only one soft thermal component (model 3) fits the observed background spectrum at a similar level of confidence. If most (or all) of the power-law component of the CXB is due to unresolved AGNs, the use of a single power-law spectral model across such a wide energy range may be incorrect. In the energy range 2–10 keV the average spectra of AGN may be represented by a power-law with the “canonical” observed α of ~ 1.7 (Mushotzky 1984; Nandra & Pounds 1994). Below this energy typical AGN spectra steepen to $\alpha \sim 2.5$ (Yuan et al. 1998) becoming no lower than ~ 2 at very faint flux levels (Hasinger et al. 1993; Almaini et al. 1996). “Type 2” (absorbed) AGN exhibit soft X-ray components, seen either in transmission or as reflection above the strongly depressed nuclear radiation (see e.g., Turner et al. 1997). Thus, the simple power-law used in the modeling is in principle inadequate and should be substituted by more complex model, such as a broken power-law. However, a broken power-law together with two thermal components model gives an insignificant improvement in fit quality to the LECS spectrum ($\Delta\chi^2 = 0.05$ for 2 additional dof).

However, a statistically acceptable fit, of similar quality as the single power-law plus two thermal components, can be obtained with a broken power-law model and a single temperature optically thin plasma giving a χ^2 of 70.0 for 63 dof (model 3, null hypothesis probability 26%). In this case the more absorbed thermal component is not required (the $\Delta\chi^2$ being 0.7 for the addition of a hard thermal component). The best-fit parameters are given in Table 4. The low-energy power-law spectral index is $\alpha_{\text{soft}} = 2.1 \pm_{0.2}^{0.3}$, while the parameter values in common with model 2 are only marginally different. The ratio between the fluxes of the thermal and non-thermal components in the 0.5–2.0 keV energy range is 0.14. The thermal component is absorbed with a low N_{H} , again consistent with an origin within the local hot bubble. Neither model 2 nor 3 requires the presence of a “super-soft” component at a temperature of $\lesssim 0.1$ keV which is commonly required to give an acceptable fit to the PSPC spectra of the soft X-ray CXB ($\Delta\chi^2 = 0.1$ for the addition of 2 dof). Miyaji et al. (1998) estimate the normalization and temperature of the “super-soft” component from observations of the Lockman Hole and Lynx-3A fields. When the PSPC temperatures of the Lockman Hole are considered, the LECS 90% confidence upper limit normalization is 6.8 in the units used by Miyaji et al. (1998). These authors determine a normalization of $9.0 \pm_{1.4}^{2.5}$ (90% confidence uncertainties). For the Lynx-3A temperature range, the LECS 90% confidence upper limit normalization is 7.9 and and the PSPC measurement 8.1 ± 0.3 .

Given that most previous spectral fits to the CXB have generally used different codes for the emission of optically thin collisionally ionized plasma (the most common be-

ing the Raymond-Smith code in XSPEC), the sensitivity of the best-fit parameters to the choice of spectral emissivity model (Raymond-Smith versus Mewe-Kaastra-Liedhal) was checked. The variations, at the present signal-to-noise ratio, are small, with differences in the best-fit temperatures of ≤ 40 and ≤ 140 eV for the soft and hard thermal components, respectively.

4. Discussion

The LECS CXB spectrum is in qualitative agreement with results obtained from PSPC and SIS spectra which are well represented by a composite spectrum consisting of a power-law and two soft thermal components. Both the slope and the normalization of the power-law component are in good agreement with previous measurements based on ASCA SIS data. The spectral index derived from the LECS data is 1.47 ± 0.10 , while values around $\simeq 1.4$ have been derived from ASCA data (Chen et al. 1997; Miyaji et al. 1998). The intercalibration of the LECS and ASCA SIS is discussed in Orr et al. (1998). The power-law index derived from the harder part of the CXB spectrum from PSPC data alone is however significantly different (1.53 ± 0.07) than the value obtained using SIS data from the same region of sky (Chen et al. 1997). These authors attribute this discrepancy to “calibration uncertainties in ROSAT”. Clearly, further comparisons of ROSAT PSPC, ASCA SIS, and BeppoSAX spectral results are desirable.

There is still no agreement on the normalization of the CXB, and the comparison is made even more difficult by the different energy bands over which the measurements have been made. The 1 keV normalization of a simple power-law fit above 1 keV in the LECS (11.0 ± 0.8 photon $\text{s}^{-1} \text{cm}^{-2} \text{keV}^{-1} \text{sr}^{-1}$) is slightly higher than observed by ASCA (9–10 photon $\text{s}^{-1} \text{cm}^{-2} \text{keV}^{-1} \text{sr}^{-1}$, Gendreau et al. 1995; Miyaji et al. 1998). This results in a 20% higher 1–2 keV flux (1.47 versus 1.22×10^{-8} erg $\text{cm}^{-2} \text{s}^{-1} \text{sr}^{-1}$). However, the LECS value is in good agreement with both the ROSAT PSPC flux (1.44×10^{-8} erg $\text{cm}^{-2} \text{s}^{-1} \text{sr}^{-1}$, Hasinger 1996) and the combined ROSAT/ASCA measurement (1.46×10^{-8} erg $\text{cm}^{-2} \text{s}^{-1} \text{sr}^{-1}$, Chen et al. 1997). We note that the 2–6 keV LECS flux is also in good agreement with that measured independently by the BeppoSAX MECS (Molendi et al. 1997).

The contribution of the power-law component in the 0.5–2.0 keV energy range is $\simeq 65\%$. This is close to the “best guess” that Hasinger et al. (1998) derive from the ROSAT deep survey results for the contribution of discrete sources of 70–80%. This fraction rises to 87% if the LECS CXB spectra is instead fit with model 3. The temperatures of the two thermal components derived from the LECS spectrum are significantly different from those obtained with the ROSAT PSPC. The best-fit LECS temperatures are $0.137 \pm_{0.022}^{0.011}$ keV and $0.7 \pm_{0.3}^{0.2}$ keV, while temperatures of 0.06 ± 0.015 keV and 0.17 ± 0.045 keV (Kerp 1994),

and ≈ 0.07 keV and ≈ 0.14 keV (Miyaji et al. 1998) are obtained with the PSPC. In addition, the CXB spectra obtained with the low-energy detectors of the A2 experiment onboard HEAO-1 can also be modeled with two thermal components with temperatures of 0.12 keV and 0.18 keV (Garmire et al. 1992).

Thus, while the component with $kT \sim 0.15$ keV is seen by both the LECS and the PSPC (and is close to the average of the temperatures obtained with HEAO 1), there is no evidence, in the LECS CXB spectra, for a very soft component with a temperature $\lesssim 0.1$ keV. A similar discrepancy is obtained when results obtained with the PSPC are compared with those from other instruments. As an example, Griffiths & Jordan (1998) compare the differential emission measures (DEM) obtained from line fluxes in Extreme Ultraviolet Explorer (EUVE) spectra of active stars with those derived by simple two temperature fits to ROSAT PSPC spectra of the same sources. While the emission measures of the hotter components appear in good agreement with the EUVE DEM, those of the cooler components are a factor $\gtrsim 10$ higher than the EUVE emission measures at the same temperature (e.g, Figs. 12–14 of Griffiths & Jordan 1998). These figures also show that there is no large disagreement between the EUVE DEM and emission measures derived from ASCA SIS and *Einstein* IPC and Solid State Spectrometer spectra. Similar results are obtained by Brickhouse & Dupree (1998) comparing the PSPC and EUVE spectra of the active binary 44 Boo. The discrepancy between the LECS and PSPC based analyses of the CXB spectrum is of the same nature, with the PSPC analysis deriving a cool component with a large emission measure, not visible in the LECS. This points to a possible systematic effect in the low-energy calibration of the PSPC.

Analysis of the LECS CXB shows that, in addition to the power-law plus two thermal components, the spectrum can also be explained with a single thermal component plus a broken power-law. The best-fit temperature for the single thermal component of 0.12 keV is very similar to the temperature of the cooler component obtained in the two temperature fit. Thus, the effect of introducing the broken power-law in the fit is to eliminate the 0.7 keV thermal component. Additional evidence for the presence of multiple components to the CXB comes from shadowing experiments using nearby (~ 60 pc) clouds such as LVC 88+36–2 and MBM 12 (Kerp 1994; Snowden et al. 1993). Differences between on- and off-cloud PSPC spectra indicate the presence of a nearby ~ 0.06 keV thermal component associated with the local hot bubble and a more distant absorbed ~ 0.17 keV thermal component located beyond the Galactic H I layer (Kerp 1994). The distant component dominates the off-cloud low-energy (< 0.3 keV) spectrum. In observations towards clouds located within the local hot bubble, the distant component suffers extra absorption, as does only part of the nearby component.

It is difficult to directly compare the LECS and PSPC spectral results. Both instruments indicate that emission from a plasma with a temperature of ~ 0.15 keV dominates the low-energy CXB spectrum. In the case of the PSPC this is the distant, absorbed, component (Kerp 1994). In contrast, the LECS indicates that this is the nearby component and the more distant (absorbed) component is either a 0.7 keV thermal plasma, or the low-energy tail of a broken power-law. If this latter model is correct, then there is no need to invoke a second thermal component. The broken power-law almost certainly results from distant AGN. The differences between on- and off-cloud spectra may result primarily from emission measure and absorption effects within the local hot bubble, as well as from additional absorption of the distant component.

5. Conclusion

We have used a set of deep observations with the BeppoSAX LECS to study the high galactic latitude CXB spectrum. We show that the spectrum is consistent with both a power-law plus two thermal components model (as currently accepted for the ROSAT PSPC plus ASCA SIS background determinations), and with a broken power-law plus single thermal component model.

While the power-law parameters are in good agreement with the ASCA SIS measurements, the temperatures of the thermal components are significantly different from those obtained with the PSPC. In particular, the “super-soft” thermal component seen by the PSPC is not evident in the LECS spectrum.

Acknowledgements. We thank G. Cusumano for providing the results of the in-flight vignetting calibration, F. Fiore and P. Giommi for discussions, and S. Molendi for the comparison with MECS results. The BeppoSAX satellite is a joint Italian-Dutch programme. M. Guainazzi, T. Oosterbroek, and A. Orr acknowledge ESA Fellowships.

References

- Almaini O., Shanks T., Boyle B.J., et al., 1996, MNRAS 282, 295
- Anders E., Grevesse N., 1989, *Geochimica et Cosmochimica Acta* 53, 197
- Bloemen J.B.G.M., 1987, ApJ 322, 694
- Boella G., Butler R.C., Perola G.C., et al., 1997, A&AS 122, 299
- Brickhouse N.S., Dupree A.K., 1998, ApJ 502, 918
- Chen L.-W., Fabian A.C., Gendreau K.C., 1997, MNRAS 285, 449
- Comastri A., Setti G., Zamorani G., Hasinger G., 1995, A&A 296, 1
- Conti G., Mattaini E., Santambrogio E.B., et al., 1994, SPIE 2279, 101
- Cusumano G., Mineo T., Guainazzi M., et al., 1999, A&A, (in prep.)
- Dickey J.M., Lockman F.J., 1990, ARA&A 28, 215

- Fiore F., La Franca F., Matt G., et al., 1998, Proc. Conf. "Science with XMM", (astro-ph/9811149)
- Garmire G.P., Nousek J.A., Apparao K.M.V., et al., 1992, ApJ 399, 694
- Gendreau K., Mushotzky R., Fabian A.C., et al., 1995, PASJ 47, L5
- Georgantopoulos I., Stewart G., Shanks T., et al., 1996, MNRAS 280, 276
- Griffiths N.W., Jordan C., 1998, ApJ 497, 883
- Hasinger G., 1992, in: The X-ray Background, Barcons X., Fabian A.C., (eds.) Cambridge University Press, Cambridge, p. 299
- Hasinger G., 1996, A&AS 120, 607
- Hasinger G., Burg R., Giacconi R., et al., 1993, A&A 275, 1
- Hasinger G., Burg R., Giacconi R., et al., 1998, A&A 329, 482
- Inoue H., Koyama K., Matusoka M., et al., 1980, ApJ 238, 886
- Jahoda K., Serlemitsos P.J., Arnaud K.A., et al., 1992, in: The X-ray Background, Barcons X., Fabian A.C. (eds.) Cambridge University Press, Cambridge, p. 240
- Jakobsen P., Kahn S.M., 1986, ApJ 309, 682
- Kerp J., 1994, A&A 289, 597
- Kerp J., Herbstmeier U., Mebold U., 1993, A&A 288, 21
- Kerp J., Burton W.B., Egger R., 1999, A&A 342, 213
- Madau P., Ghisellini G., Fabian A.C., 1993, ApJ 410, L7
- Marshall F.E., Boldt E.A., Holt S.S., et al., 1980, ApJ 235, 4
- McCammon D., Sanders W.T., 1990, ARAA 28, 657
- McCammon D., Burrows D.N., Sanders W.T., Kraushaar W.L., 1983, ApJ 269, 107
- Mewe R., Gronenschild E.H.B.M., van den Oord G.H.J., 1985, A&AS 62, 197
- Mewe R., Lemen J.R., van den Oord G.H.J., 1986, A&AS 65, 511
- Miyaji T., Ishisaki Y., Ogasaka Y., et al., 1998, A&A 334, L13
- Molendi S., Chiappetti L., Cusumano G., et al., 1997, Mem. Soc. Astron. Ital. 68 n.1/2, 113
- Morisson D., McCammon D., 1983, ApJ 270, 119
- Mushotzky R.F., 1984, Advances Sp. Res. 3, 10
- Nandra K., Pounds K.A., 1994, MNRAS 268, 405
- Orr A., Yaqoob T., Parmar A.N., et al., 1998, A&A 337, 685
- Parmar A.N., Martin D.D.E., Bavdaz M., et al., 1997, A&AS 122, 309
- Parmar A.N., Oosterbroek T., Orr A., et al., 1999, A&AS in press, (astro-ph/9902075)
- Rocchia R., Arnaud M., Blondel C., et al., 1984, A&A 130, 53
- Setti G., Woltjer L., 1989, A&A 224, L21
- Snowden S.L., McCammon D., Verter D., 1993, ApJ 409, L21
- Snowden S.L., Hasinger G., Jahoda K., et al., 1994, ApJ 430, 601
- Snowden S.L., Freyberg M.J., Plucinsky P.P., et al., 1995, ApJ 454, 643
- Snowden S.L., Egger R., Freyberg M.J., et al., 1997, ApJ 485, 125
- Turner T.J., George I.M., Nandra K., Mushotzky R.F., 1997, ApJS 113, 23
- Yuan W., Brinkmann W., Siebert J., Voges W., 1998, A&A 330, 108